VELOCITY MODELING TO DETERMINE PORE ASPECT RATIOS OF THE HAYNESVILLE SHALE.

Kwon Taek Oh

Department of Geological Sciences
The University of Texas at Austin

ABSTRACT

This work estimates pore shapes from seismic velocity in the Haynesville Shale. The effective elastic moduli and velocities of the matrix were calculated using the self-consistent model. The Backus average was used to upscale the high-frequency well log data to the low-frequency seismic scale. Comparing calculated velocities from the self-consistent model to upscaled Backus velocities with a convergence of 0.5% made it possible to determine pore aspect ratios versus depth at 20 Hz and 50 Hz. The effects of pore fluid property changes were studied by comparing velocities between the self-consistent model and Gassmann substitution for various types of fluid saturations. P-wave velocities calculated by the self- consistent model for patchy saturation cases have larger values than those from Gassmann fluid substitution, but S-wave velocities were very similar. Pore aspect ratios for various fluid property types were also calculated. Pore aspect ratios determined for the patchy saturation cases were the smallest, and those for the uniform saturation cases were the largest. Pore aspect ratios determined for the patchy saturation cases varied from 0.035 to 0.296 with a mean of 0.145. These are considered the most reasonable values for the Haynesville Shale in consideration of water and partial gas saturation.

INTRODUCTION

The shapes of pores in sedimentary rocks affect both the transport and elastic properties of that rock (Sun, 2004; Avseth et al., 2010; Sondergeld et al., 2010). Typically, rounded pores correspond to faster seismic velocity. Counter to that, thin, elongated pores often lead to slower velocity. Therefore, the relationship between the pore shape and the elastic properties is important to understand. The work here characterizes pore shapes in terms of velocities calculated from rock physics relationships for the Haynesville Shale.

New techniques such as horizontal drilling and hydraulic fracturing make the production of shale gas feasible in spite of extremely low permeability, on the order of nanoDarcies. The purpose of the fracturing is to connect isolated pores and natural fractures with one another to enhance the permeability for economic production. The Haynesville Shale has penny-shaped or elongated grains compared with the other shale formations (Curtis et al., 2010). In this study, pore aspect ratios were determined by comparing measured velocities from well data to modeled velocities computed from the self-consistent model, which incorporates grain and pore shapes into the formulation (Mavko et al., 2009). This comparison was evaluated at the scale of the well

data and on upscaled data. By determining pore aspect ratios of the formation, we can better understand elastic properties of the Haynesville Shale. By performing this on up-scaled data, we can also estimate the ability to infer pore shape from seismic data.

The well log data used in this study are from the Haynesville Shale, which is a black, organic-rich shale of upper Jurassic age that underlies much of the Gulf Coast area. It was deposited about 150 million years ago in a shallow offshore environment. The Haynesville Shale is underlain by the Smackover Formation and overlain by rocks of the Cotton Valley Group (Hammes et al., 2009). Because of its low permeability, the Haynesville was originally considered to be a gas source rock rather than a gas reservoir. Natural gas production from the Haynesville is one of the largest gas reservoirs in United States, which occurs from rocks about 10,000 to 13,000 feet subsurface in northwest Louisiana and east Texas.

Figure 1a is a nano-scale image of the Haynesville Shale. Dark patches in the red ellipses are pieces of organic material (solid) inside of pores. Light gray features in the white ellipses are matrix or grains. Most pore shapes are flat (or crack-like), which have small aspect ratios. Grain shapes vary in this formation. Figure 1b is an image showing the variability of pore type in the Haynesville. On the middle right, numerous nano-scale pores and one μm-scale pore are present (o). At the lower left (ip), a number of pores (inter-crystalline pores) are present between pyrite framboid crystals. In the top center (M), pores are present between organic matter and mineral grain.

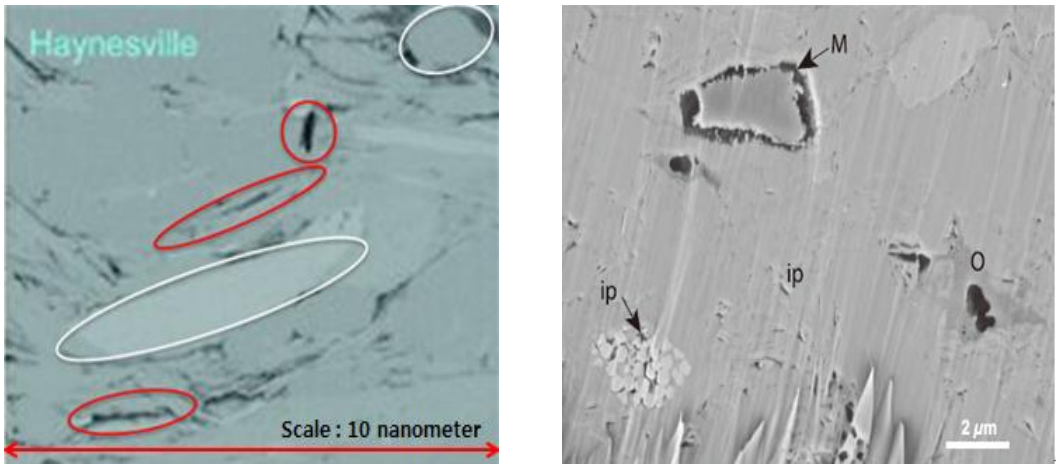

(a) **(b)**

Figure 1. (a) Nano-scale image of the Haynesville Shale (Modified from Curtis et al, 2010) (b) SEM image showing different pore types of the Haynesville including organic (o), interparticle (ip), and moldic (M) micropores and nanopores (Hammes et al., 2011).

Figures 2 and 3 are the well log data from the Haynesville Shale including gamma ray (API), density (g/cc), density porosity (%), P-wave velocity (km/s), and S-wave velocity (km/s) versus depth.

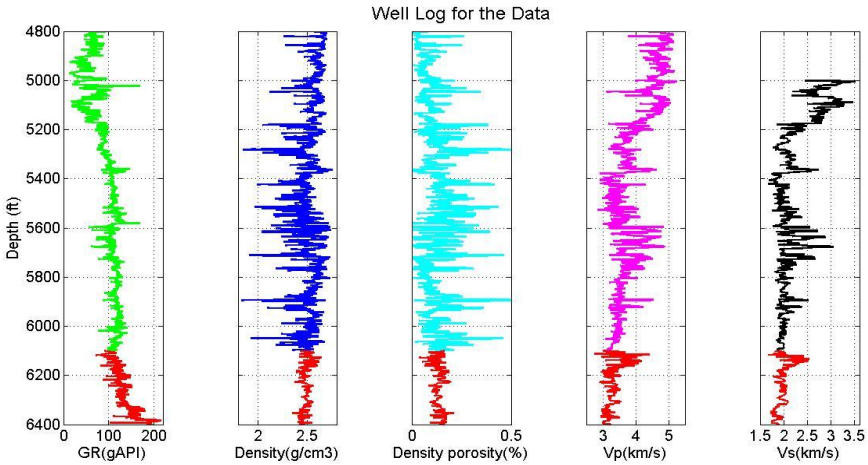

Figure 2. Well log data. From the left, gamma ray (API), density (g/cc), density porosity (%), P-wave velocity (km/s), and S-wave velocity (km/s) are plotted versus depth. The Haynesville Shale in this well is colored by red at the bottom of the figure. The vertical axis is artificial depth.

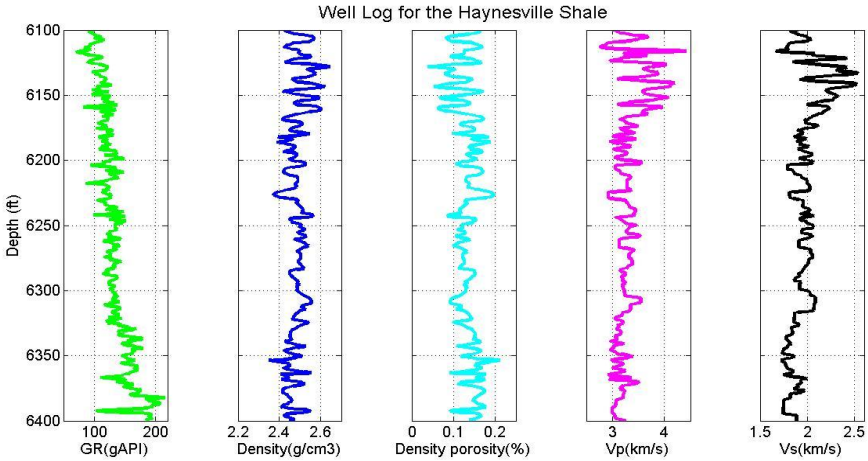

Figure 3. Well log data from the Haynesville Shale, showing the red portions of the curves from Figure 2.

The Haynesville Shale has higher gamma ray (API) values relative to the overlying formation because the Haynesville contains a larger percentage of clays (average 35.6 %). Also, it has higher porosity, lower density and velocities than the overlying formation on account of clay and kerogen content. P-wave and S-wave velocities are inversely correlated with the gamma ray, and are highly correlated with the density. In the Haynesville Shale, P-wave velocity varies from 2.75 to 4.42 km/s (average 3.28 km/s) and S-wave velocity ranges over 1.67 - 2.53 km/s (average 1.96 km/s). The range of bulk density is 2.35 through 2.65 g/cc with the average of 2.48 g/cc. P-impedance changes over 6.67 to11.03 g/cc*km/s with the average of 8.14 g/cc*km/s. The upper part of the Haynesville Shale has higher P-wave velocity (km/s) and S-wave velocity (km/s) than deeper sections. From this information, we interpret that the shallower intervals of the Haynesville contain less clay than the deeper intervals.

Figure 4 shows the relationship between seismic velocities and reservoir properties of the Haynesville Shale. Those are cross plots for Vp versus Vs, P-impedance versus Vp/Vs, Vp

versus porosity, and Vs versus porosity, respectively. Data points are colored by gamma ray. P-wave and S-wave velocities are highly correlated and have large changes with little changes in porosity. The general velocity trends of the Haynesville Shale increase with decreasing porosity and clay contents. Red indicates high clay content in Figure 4.

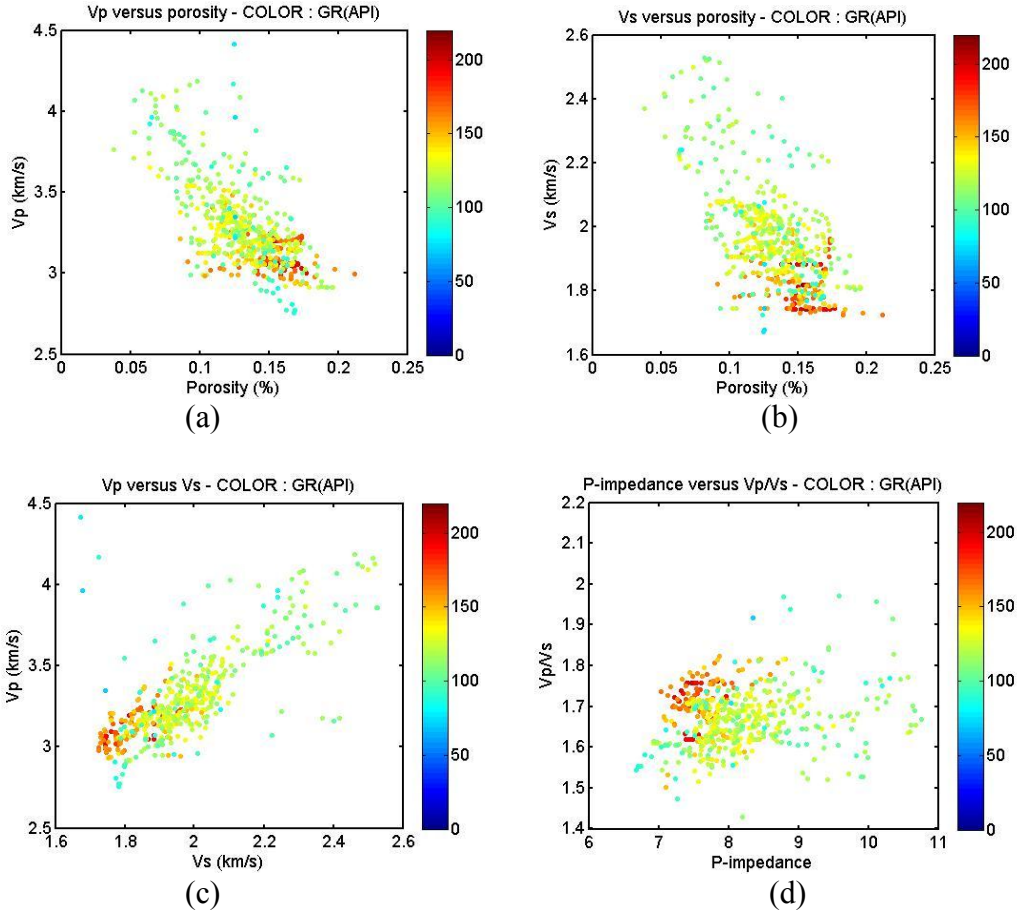

Figure 4. Cross plots of the Haynesville Shale. (a) Vp versus porosity (b) Vs versus porosity (c) Vp versus Vs (d) P-impedance versus Vp/Vs. Data points are colored by gamma ray. High clay contents are in red.

THEORY

Effective media theory

Sonic log data can include large fluctuations in P- wave and S- wave velocities because they are measured at high frequencies (approximately 10 kHz) approximately every 15 cm within the wellbore. These fluctuations are significantly decreased at lower frequencies (below 100 Hz) because the wavelength is much larger than at the well log scale. Because of different measurement scales for data, we need to upscale well log data to the seismic scale. Then we can understand how elastic properties and estimated rock properties appear at the seismic scale. Upscaling means theoretically predicting the elastic properties in rocks at lower frequency from higher frequency sonic logging data (Bayuk et al., 2007). When the wavelength (λ) is large

compared to the layer thickness (d), the wave velocity is given by an average of the properties in the individual layers (Backus, 1962). The waves behave as if propagating in an effective isotropic homogeneous medium even though the medium may be anisotropic. The Backus average represents the low-frequency limit. When λ / d >> 1, a stratified medium behaves as a homogeneous effective medium with wave propagation normal to the layering. The equations that describe this are

$$V_{EMT} = \left(\frac{M_{EMT}}{\rho_{ave}}\right)^{1/2} \tag{1}$$

The effective velocity, V_{EMT}, is calculated using the Backus average of the elastic stiffness tensors C_{ij} of the constituents. For normal incidence propagation, this is equivalent to the Reuss average or iso-stress average of the P-wave modulus.

$$M_{EMT} = \left[\sum_k \frac{f_k}{M_k}\right]^{-1} \text{ or } \frac{1}{\rho_{ave} V_{EMT}^2} = \sum_k \frac{f_k}{\rho_k V_k^2} \tag{2}$$

$$\rho_{ave} = \sum_k f_k \rho_k \tag{3}$$

Where, f_k is the fractional thickness, ρ_k are layer densities, M_k are layer moduli, and V_k are velocities of each layer. The Backus average can be calculated using a moving window, where a stack of thin layers is approximated by the properties of a single thick layer.

In this study, I used two frequencies, 20 Hz and 50 Hz, to calculate a moving average as a function of depth. These two frequencies were selected because they are in the bandwidth (10 – 100 Hz) of surface seismic data. Figure 5 is the moving Backus averages of P-wave and S-wave velocities and Figure 6 is the moving arithmetic averages of density and porosity for 20 and 50 Hz, respectively.

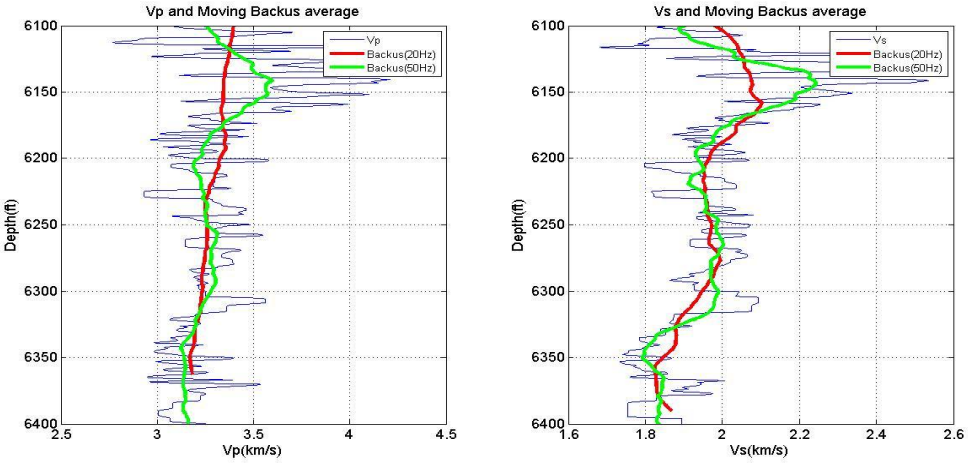

Figure 5. Moving Backus average for 20 Hz and 50 Hz. From the left to right, moving Backus averages for P-wave velocity (km/s) and S-wave velocity (km/s) are plotted versus depth.

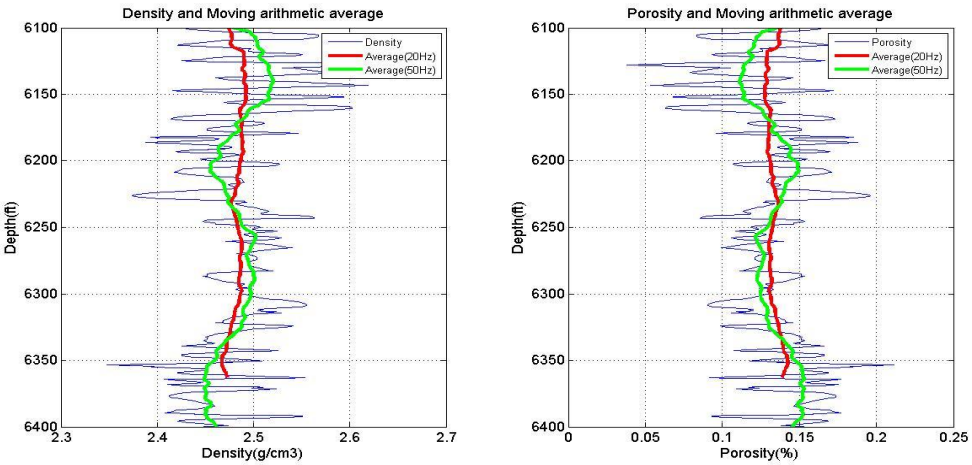

Figure 6. Moving arithmetic average for 20 Hz and 50 Hz. From the left to right, moving arithmetic averages for density (g/cc), and porosity are plotted versus depth.

Self-consistent model

To estimate the effective moduli of a composite or porous elastic material for the Haynesville Shale, we need to know the elastic properties and the volume fractions of the individual components, and the geometric details of the shapes and spatial distributions of the components (Mavko et al., 2009). The self-consistent model used in this study is the method to extend these geometric details to relatively high concentrations of inclusions. It is able to model multiple mineral phases for idealized ellipsoidal pores. Avseth et al. (2010) indicated that inclusion models such as the self-consistent model approximate the rock as an elastic solid containing inclusions that represent the pore space.

Figure 7 is a schematic diagram of the self-consistent model. The square represents an infinite background matrix and the circle does a rock. Inside the rock, blue and black ellipses represent isolated mineral grain inclusions and pore inclusions, respectively. Isolated mineral grains and pore inclusions with various aspect ratios in the rock were assumed to be imbedded in an infinite background matrix. The aspect ratio (a) of an ellipsoid is defined as the ratio between its smallest and largest axes.

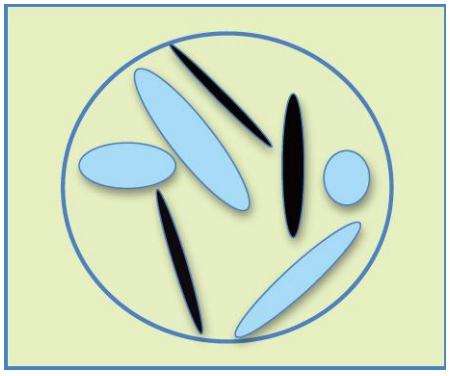

Figure 7. Schematic diagram of the self-consistent model. The square represents an infinite background matrix and the circle does a rock. Blue and black ellipses represent mineral grain inclusions and pore inclusions in the rock, respectively (Jiang and Spikes, 2011).

Pore aspect ratio estimation

The elastic properties of the solid grains and pores affect the elastic moduli of the rock. The effective moduli of the infinite background matrix can be solved by simultaneous iteration. Berryman (1980) introduced a general form of the self-consistent model for N-phase composites (Mavko et al., 2009).

$$\sum_{i=1}^{N} x_i(K_i - K_{SC}^*)P^{*i} = 0 \tag{4}$$

$$\sum_{i=1}^{N} x_i(\mu_i - \mu_{SC}^*)Q^{*i} = 0 \tag{5}$$

Where i refers to the i^{th} material, x_i is its volume fraction of each phase of the rock, and P and Q are geometric factors. In this equations, K^{*SC} and μ^{*SC} are the effective bulk and shear moduli, respectively, of a cracked medium with randomly oriented penny-shaped cracks to be calculated. In equations 4 and 5, P and Q for penny cracks are

$$P^{*i} = \frac{K_m + \frac{4}{3}\mu_i}{K_i + \frac{4}{3}\mu_i + \pi\alpha\beta_m} \tag{6}$$

$$Q^{*i} = \frac{1}{5}\left[1 + \frac{8\mu_m}{4\mu_i + \pi\alpha\beta(\mu_m + 2\beta_m)} + 2\frac{K_i + \frac{2}{3}(\mu_i + \mu_m)}{K_i + \frac{4}{3}\mu_i + \pi\alpha\beta_m}\right] \tag{7}$$

$$\beta = \mu\left[\frac{(3K+\mu)}{(3K+4\mu)}\right] \tag{8}$$

where a is the pore aspect ratio. In the self-consistent model, the pores are isolated, and the fluids cannot move between the pores. Therefore, the model is considered a high-frequency model most appropriate to model ultrasonic laboratory conditions because there is no time for wave-induced pore pressure to equilibrate. The Haynesville Shale has very low permeability and mostly isolated pores. The fluid effect on the modeled velocities is analyzed in this study.

Figure 8 shows cross plots of P-wave velocity, S-wave velocity, bulk modulus, and shear modulus versus total porosity for the Haynesville Shale using the self-consistent model with measured data. Elastic properties of fluids in the pore spaces were fixed values (Bulk modulus: 1 GPa and density: 0.8 g/cc for fluids). In the model, 50 pore inclusions in the rock were assumed. The aspect ratios for the pore inclusions were assumed with mean 0.145, and normally distributed with standard deviation 0.01. An average composition within whole range of the formation was used. Bulk and shear moduli of in-situ data were calculated from Equations 9 and 10.

$$K = \rho_{bulk}\left(V_p^2 - \frac{4}{3}V_s^2\right) \tag{9}$$

$$\mu = \rho_{bulk}(V_s^2) \tag{10}$$

The blue lines are modeled velocities calculated from the self-consistent model. Data are colored by gamma ray. These plots show the trend that effective bulk moduli, shear moduli, and P-wave velocities modeled from the self-consistent model decrease while total porosity increases. These calculated results are similar to measured data values and cross almost the center of the data. Therefore, the self-consistent approximation characterizes the overall trend observed in the data from the Haynesville Shale.

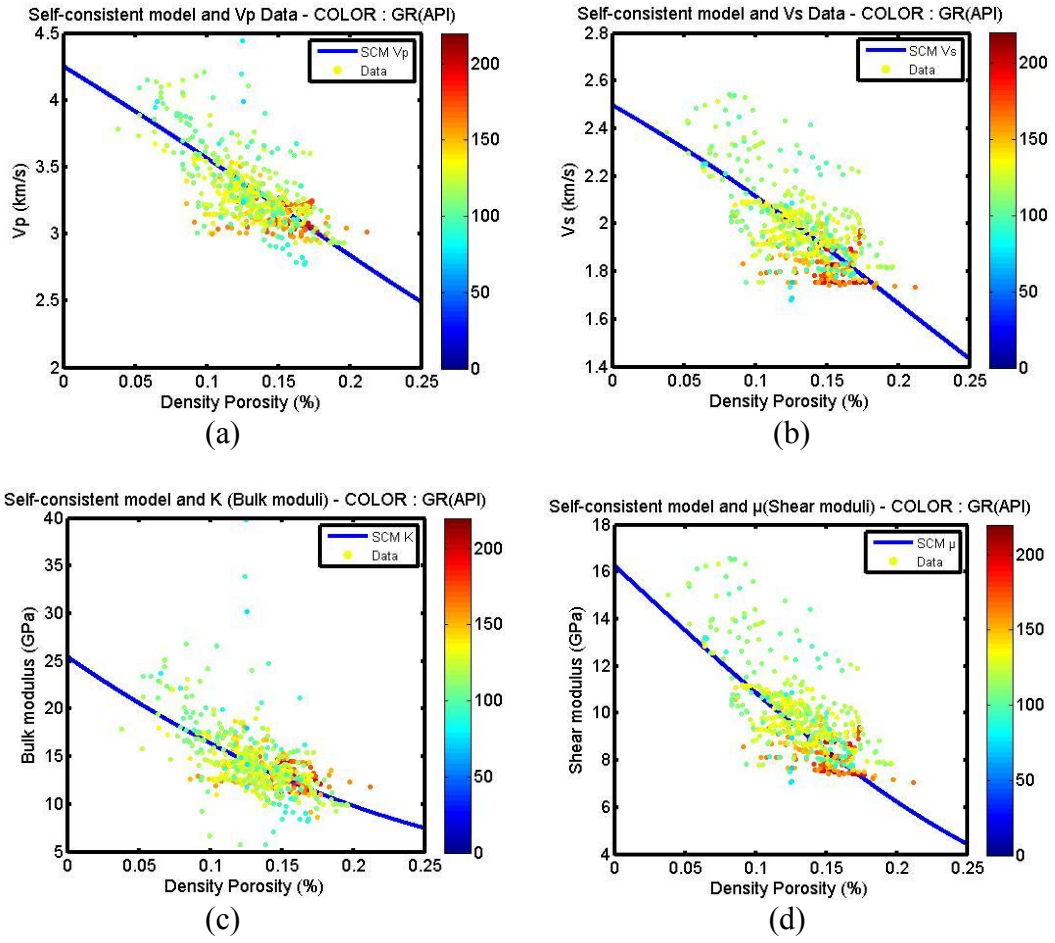

Figure 8. Cross plots of (a) Vp versus porosity, (b) Vs versus porosity, (c) bulk modulus versus porosity, and (d) shear modulus versus porosity data overlain with the self-consistent modeling results for the Haynesville Shale. Data points are colored by gamma ray. The colored lines are results of the self-consistent model with average composition and fixed pore aspect ratio of the Haynesville Shale.

Fluid mixture with partial saturation

Knight and Nolen-Hoeksema (1990) and Berryman et al. (1999) demonstrated that laboratory data being collected during a continuous imbibition/drainage experiment showed a clear

dependence of elastic wave velocities on the detail of the pore-scale distribution of water and air in the rock. Figure 9 shows the hysteresis effect between the imbibition and drainage experiments. This effect becomes significant in the higher saturation region (Sw > 0.8) where both Vp and Vs increased rapidly to higher values.

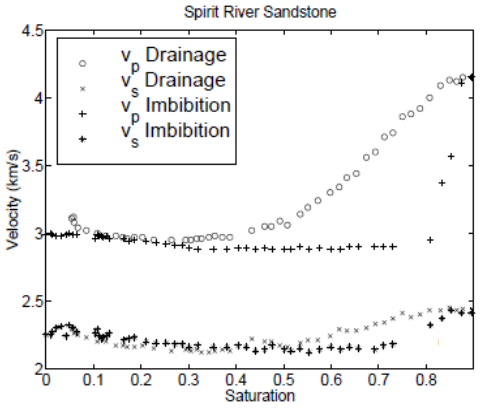

Figure 9. Vp and Vs versus Sw measured during a continuous imbibition/drainage experiment (Berryman et al., 1999).

From this result, it is apparent that elastic velocities can be significantly affected by the pore scale configuration of fluids. Therefore, velocities depend on both saturation and the fluid mixing scales (Avseth et al., 2005). The imbibition is typical when phases are mixed at a fine scale (uniform saturation). On the other hand, the drainage is typical when the phases are mixed at a coarse scale (patchy saturation). The patchy and uniform saturation curves are upper and lower bounds in fluid mixing scales. The uniform saturation model is typically used for reservoirs with oil and water cases. Reservoirs with gas are very likely to show patchy behavior. The patchy saturation upper bound can be found by the Voigt average and the uniform saturation lower bound can be calculated by the Reuss average of the fluid modulus, respectively (Mavko et al., 2009).

$$K_{fl} = \sum S_i K_i \tag{11}$$

$$\frac{1}{K_{fl}} = \sum \left(\frac{S_i}{K_i}\right) \tag{12}$$

In Equations 11 and 12, K_{fl} is the effective bulk modulus of the fluid mixture, K_i is the bulk moduli of the individual fluid phases, and S_i represents their saturations. Mavko and Mukerji (1998) showed that patchy saturation always lead to higher seismic velocities than if the same fluids are mixed uniformly at a fine scale.

Gassmann fluid substitution

Gassmann fluid substitution allows us to obtain the bulk and shear modulus of the fluid-saturated rock from the dry rock and mineral modulus, porosity, and fluid modulus. This can be done under the assumptions that the rock is isotropic, the mineral modulus is homogeneous, and

the frequency is low. High frequencies, high fluid viscosity, and large fractions of clay can violate these assumptions. This theory predicts that the rock's bulk modulus (K) changes with saturation, but the shear modulus (G) remains fixed between dry and saturated rocks. P-waves are sensitive to pore fluids while, except for density, S-waves are not. Gassmann (1951) provided this general relation between the dry rock and saturated-rock moduli.

$$\frac{K_2}{K_{min}-K_2} - \frac{K_{fl2}}{\varphi(K_{min}-K_{fl2})} = \frac{K_1}{K_{min}-K_1} - \frac{K_{fl1}}{\varphi(K_{min}-K_{fl1})} \tag{13}$$

Equation (13) also can be written as:

$$\frac{K_{sat}}{K_{min}-K_{sat}} = \frac{K_{dry}}{K_{min}-K_{dry}} + \frac{K_{fluid}}{\varphi(K_{min}-K_{fluid})}\ ,\ \frac{1}{\mu_{sat}} = \frac{1}{\mu_{dry}}. \tag{14}$$

Closing stress

A pore with a given aspect ratio at the depth can be open or closed according to the matrix material and the closing stress. A relationship between the closing stress and the aspect ratio is defined in Equation 15 (Mavko et al., 2009).

$$\sigma_{close} = \frac{3\pi(1-2\nu_0)}{4(1-\nu_0{}^2)}\sigma K_0 \tag{15}$$

The closing stress for a single isolated pore in an infinite homogeneous matrix with Poisson's ratio (v_0) and bulk modulus (K_0) are plotted in Figure 10. Matrix compositions are quartz, clay, and average compositions of the Haynesville Shale. The confining pressure of the formation in each depth is calculated by Equation 16 (Castagna and Backus, 1993).

$$P_c = \int_{h_0=0}^{h_0} \rho g dh \tag{16}$$

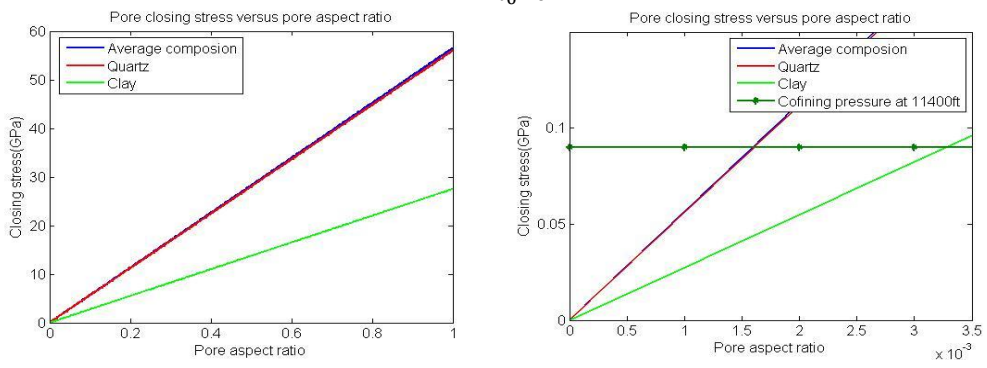

(a) (b)

Figure 10. (a) The closing stress of a single isolated pore versus various pore aspect ratios. (b) Zoom of (a). When the pore aspect ratio is 1, the closing stress of a single isolated pore with a quartz matrix is about 55 GPa. The closing stress with a clay matrix is less than 30 GPa, and the closing stress for an average composition of the Haynesville Shale is almost the same pure quartz. At the top and the bottom of the Haynesville Shale, the confining pressure is 85 MPa and 90 MPa, respectively.

The confining pressure of the Haynesville Shale varies over 85 to 90 MPa. For quartz and average composition of the Haynesville Shale, the pore aspect ratios that are closed are 0.0015 to 0.0016 at the top and bottom of the Haynesville Shale, respectively. For the clay matrix, closed pores have aspect ratios at 0.0035. The closing stresses are also affected by pore pressure. As pore pressure increases, effective pressure decreases, and small crack-like pores could open.

METHODOLOGY TO DETERMINE PORE ASPECT RATIOS

Effective elastic moduli were calculated using the self-consistent model with component composition data and an estimated pore aspect ratio. XRD analysis data (48 samples) (Hammes, 2010) versus depth were used as component composition data in the modeling. These 48 samples were from depth locations throughout the Haynesville and Bossier Shale, which is the overlying formation of the Haynesville. XRD data have 28 composition samples in the Haynesville shale, and the distance between analyzed data was approximately 10 feet (3.05 m) in depth. Using those calculated effective elastic moduli, P-wave and S-wave velocities were calculated at each depth of the formation. P-wave velocities calculated by the self-consistent model were compared to up-scaled P-wave velocities from the moving Backus average. S-wave velocities were not used in this modeling due to inherent uncertainties in both the measurements and model calculations. This is a typical iteration method by trial and error. When the difference was within 0.5 %, the aspect ratio used in the modeling was determined at each location (Figure 11). After determining the pore aspect ratios for the depths with XRD data, component compositions between depths were interpolated. From the 28 XRD data of the Haynesville shale, I interpolated compositions between the depths twice. As a result, 109 composition data throughout the Haynesville were modeled in total. Then the aspect ratios were estimated for the entire formation using the same procedure. By interpolating composition data between depths, the aspect ratios determined in the modeling became more specific versus depth than the original values. This helped to understand elastic properties according to the effect of compositions and pore aspect ratios at the seismic scale.

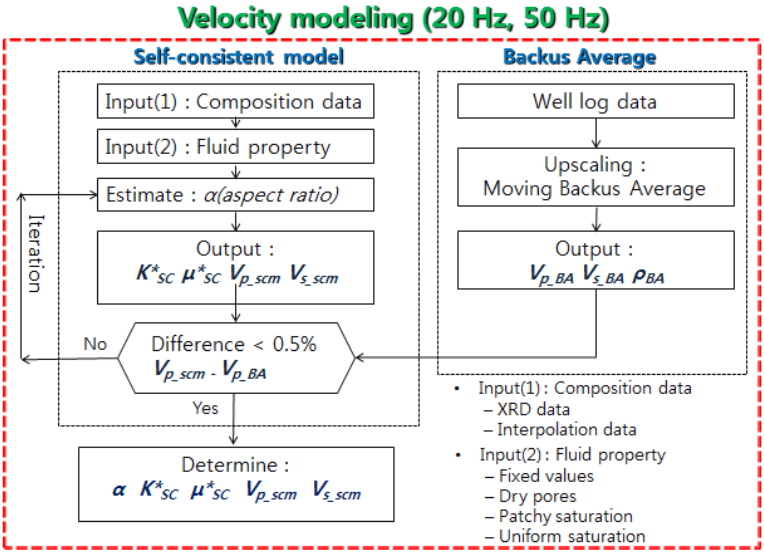

Figure 11. Flow chart of velocity modeling to determine the pore aspect ratio of specific depth in the Haynesville Shale. This modeling was performed for the entire depth range at both 20 Hz and 50 Hz. At first, bulk modulus (1 GPa) and density (0.8 g/cc) values for pore fluids were fixed. Partial saturation cases are dealt with in later sections.

This method was carried out for 20 Hz and 50 Hz moving Backus averages velocities to determine the dependency of the frequency for the modeling. At first, this calculation was carried out with constant fluid elastic properties to minimize the effect of pore fluid change. Then the effects of fluid property changes were included. Figure 11 explains the modeling procedure to determine the pore aspect ratios and the effective elastic moduli of the specific depth.

	Bulk Modulus (GPa)	Shear Modulus (GPa)	Density (g/cm^3)		Bulk Modulus (GPa)	Shear Modulus (GPa)	Density (g/cm^3)
Quartz	36.6	45	2.65	Kerogen	2.9	2.7	1.3
Feldspar	37.5	15	2.62	Clay	18	7	2.58
Calcite	69	33	2.71	Water	2.8	0	1.09
Dolomite	95	45	2.87	Gas	0.07	0	0.16
Pyrite	147.3	132.5	4.93				

Table 1. Elastic pore properties of minerals used in this modeling (Simmons and Birth, 1963; Carmichael, 1989; Mavko et al., 2009).

RESULTS AND DISCUSSION

Results of velocity modeling

The results of the estimated pore aspect ratios for the 20 Hz and 50 Hz cases for the original XRD data and interpolated data are shown in Tables 2 and 3, and Figures 12 and 13, respectively. Calculated pore aspect ratios of the interpolated data for 20 Hz vary from 0.029 to 0.320 with the mean of 0.144 and the range of pore aspect ratios of the interpolated data for 50 Hz is from 0.035 to 0.298 with the average of 0.143 (Figure 12). The aspect ratios for 20 Hz and 50 Hz are similar, but the log of pore aspect ratios for 50 Hz shows a narrower range and a smoother variation versus depth than that of 20 Hz. For 50 Hz, the velocities show a sharp change between depths compared to that of 20 Hz. However, it appears that the variation of velocities and pore aspect ratios are inversely related in the self-consistent model. The histograms for the interpolated data appear to be normally distributed, but some of the histograms for the original XRD data appear uniformly distributed.

Pore aspect ratios		Vp_backus	Vs_backus	K_scm	Miu_scm	Vp_scm	Vs_scm	Vp Diff (%)	Vs Diff (%)
Max	0.320	3.3832	2.0994	16.5155	10.0225	3.3889	2.0213	0.47	8.90
Min	0.029	3.1696	1.8251	12.4748	7.8768	3.1586	1.8540	-0.50	-2.88
Mean	0.144	3.2810	1.9739	13.6729	8.9453	3.2816	1.9398	-0.02	1.67

Table 2. The maximum, minimum and mean values of estimated pore aspect ratios and calculated effective elastic moduli for 20 Hz for the interpolated composition data. From the left, estimated pore aspect ratios, P-wave and S-wave velocities calculated from the Backus average, bulk moduli, shear moduli, P-wave and S-wave velocities calculated from the self-consistent model, differences of P-wave and S-wave velocities between the Backus average and the self-consistent model, respectively.

Pore aspect ratios		Vp_backus	Vs_backus	K_scm	Miu_scm	Vp_scm	Vs_scm	Vp Diff (%)	Vs Diff (%)
Max	0.298	3.591319	2.240998	17.9875	11.4649	3.6039	2.1626	0.46	5.53
Min	0.035	3.121977	1.793293	12.1049	7.6508	3.1221	1.8288	-0.46	-2.66
Mean	0.143	3.288928	1.97442	13.7074	9.013779	3.288696	1.946185	0.01	1.35

Table 3. The maximum, minimum and mean values of estimated pore aspect ratios and calculated effective elastic moduli for 50 Hz for the interpolated data.

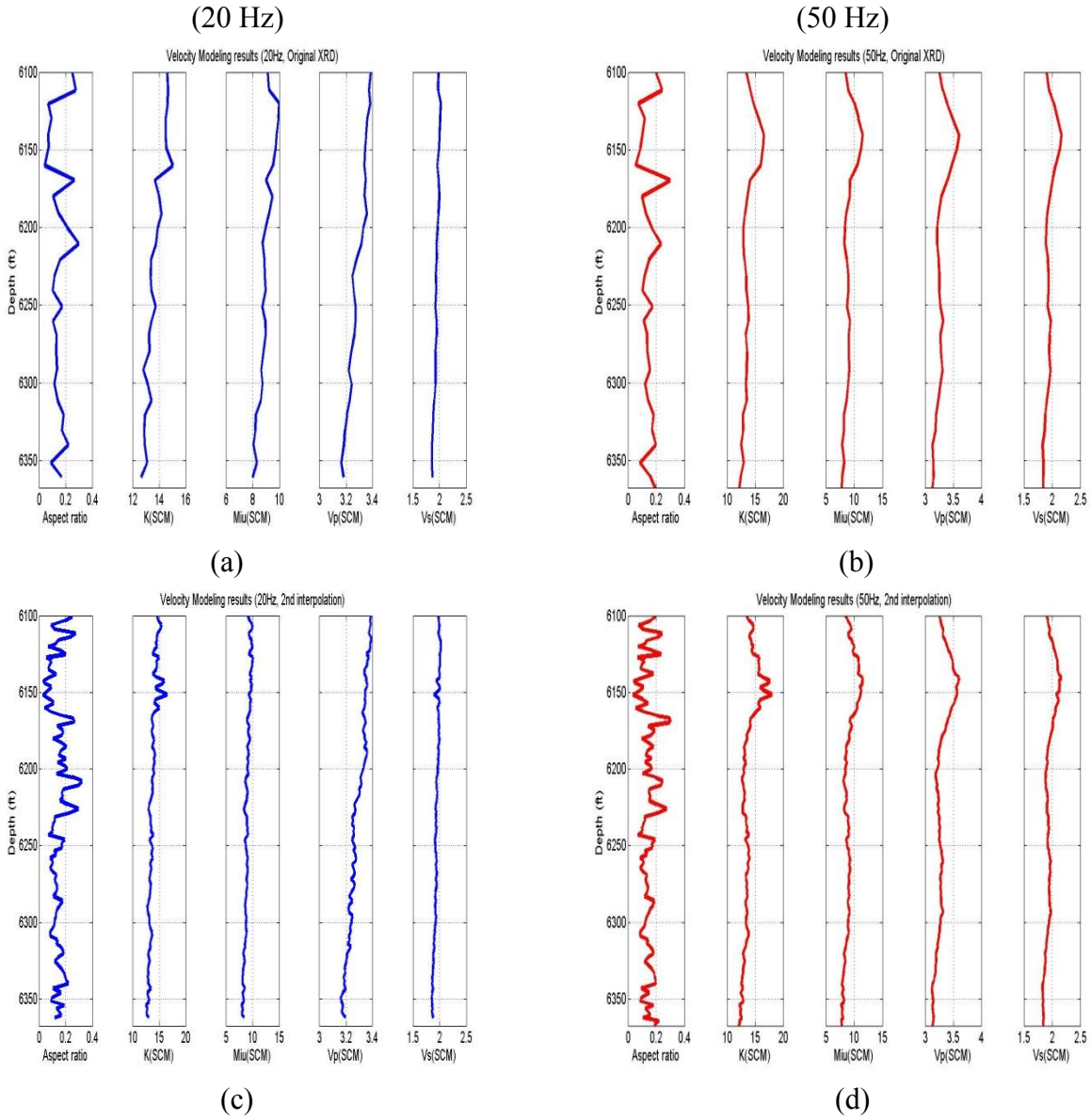

Figure 12. Estimated pore aspect ratios from velocity modeling for 20 Hz and 50 Hz. (a) 20 Hz, original XRD data, (b) 50 Hz, original XRD data, (c) 20 Hz, the interpolated data, and (d) 50 Hz,

the interpolated data. In each Figure, from the left, pore aspect ratios, effective bulk and shear moduli, effective P-wave and S-wave velocities calculated by the self-consistent model.

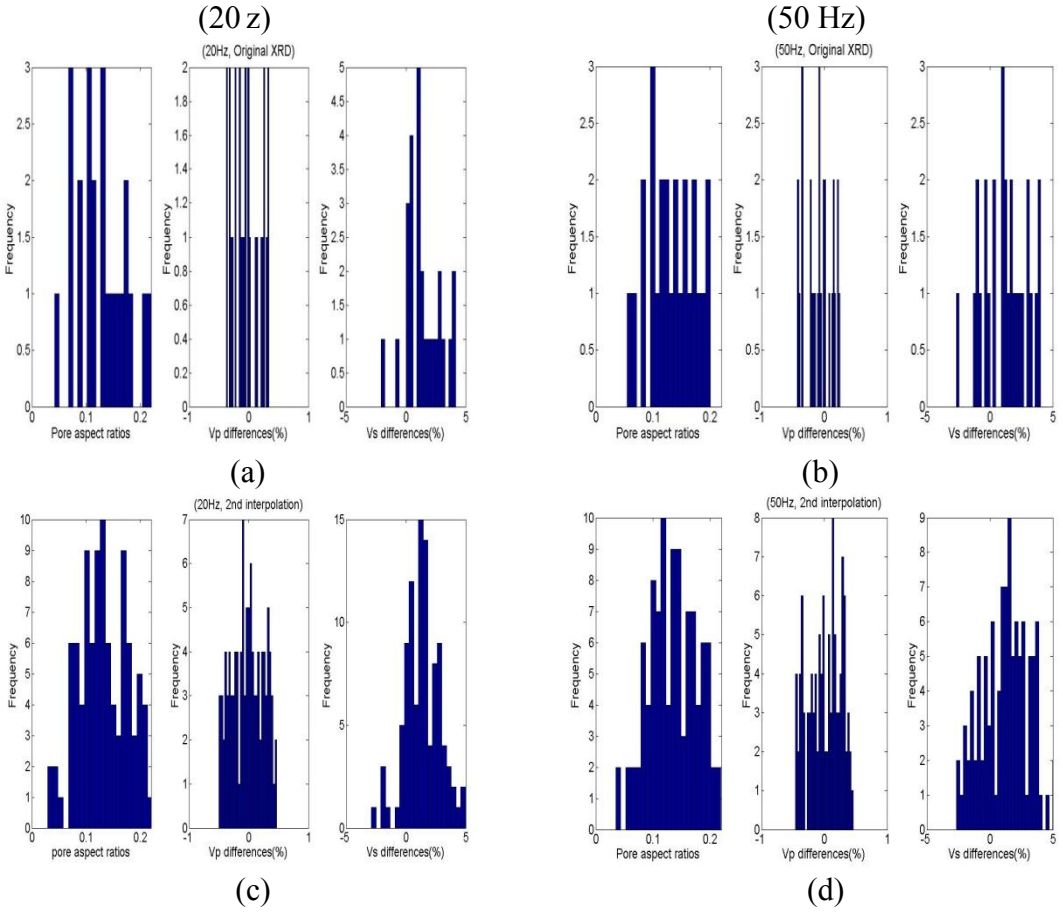

Figure 13. The histograms of estimated pore aspect ratios for 20 Hz and 50 Hz. (a) 20 Hz, original XRD data, (b) 50 Hz, original XRD data, (c) 20 Hz, the interpolated data, and (d) 50 Hz, the interpolated data. In each frame, from the left, pore aspect ratios, differences of P-wave and S-wave velocities between the Backus average and the self-consistent model.

To compare the respective histograms in Figure 13, Q-Q plots were generated. A Q-Q plot is a plot of the quantiles of two distributions. In statistics, a Q-Q plot is a probability plot, which is a graphical method for comparing two probability distributions by plotting their quantiles against each other (Wilks, 2011). The pattern of points in the plot is a quantitative comparison between the two distributions. If the two distributions being compared are similar, the points in the Q-Q plot will approximately lie on the one-to-one line. A Q-Q plot is generally a more powerful approach to comparing two data distributions than comparing histograms of the two samples.

In addition, correlation coefficients for pore aspect ratios, Vp and Vs differences between original XRD data and interpolated data are 0.9987, 0.9545, and 0.9985, each. From the results of Q-Q plots and correlation coefficients, it is possible to argue that the interpolated data to be analyzed in this modeling have similar distributions to the original XRD data. Therefore,

velocity modeling to determine the pore aspect ratios in the Haynesville shale is reasonable for the original XRD data as well as the interpolated data.

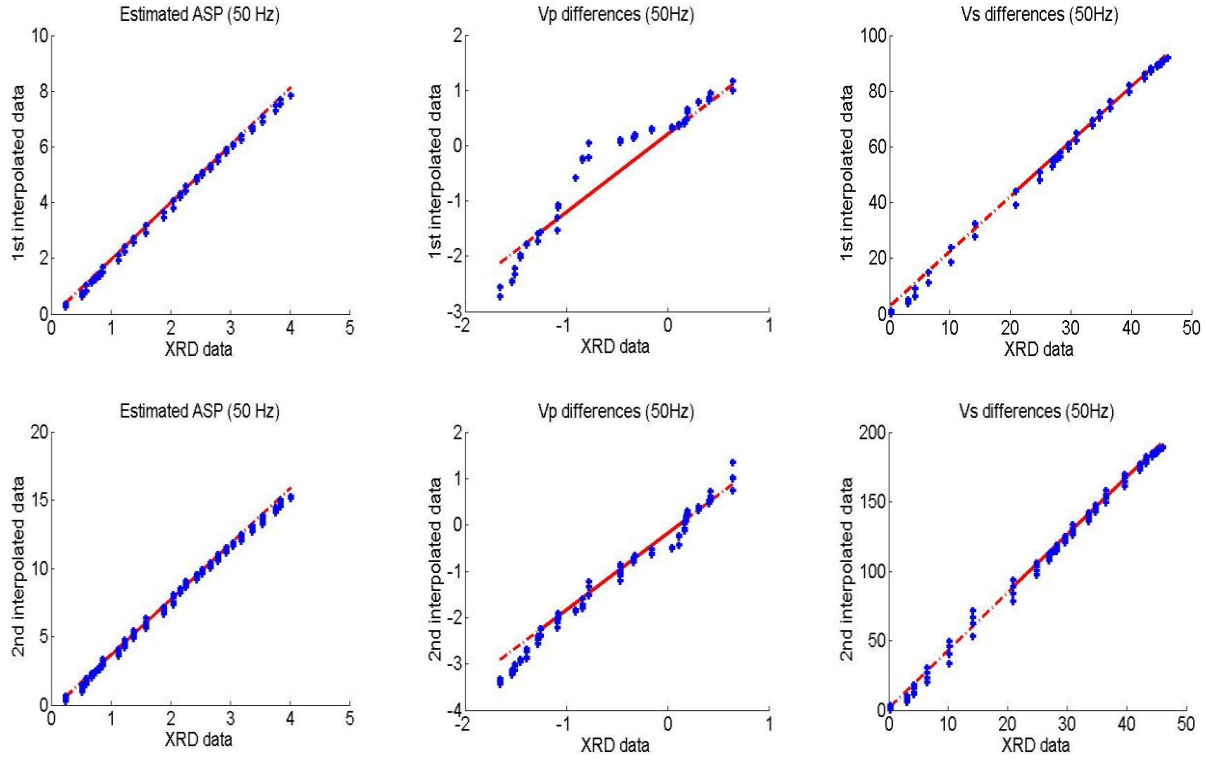

Figure 14. The Q-Q plots between original XRD data and interpolated data from the velocity modeling for 50 Hz. The upper figure is the Q-Q plot between original XRD and 1st interpolated data, and the bottom one is between the original XRD and 2nd interpolated data. In each Q-Q plot, from the left, pore aspect ratios, differences of P-wave and S-wave velocities between the self-consistent model and the Backus average are plotted.

The effects of fluid property changes to velocities

Patchy saturation and uniform saturation

After estimating pore aspect ratios for constant fluid properties in the Haynesville shale, the next step was to analyze the effect of pore-fluid properties. To analyze this effect, I performed simulations for five cases, which are the dry pores, patchy saturation, and uniform saturation cases for the self-consistent model and Gassmann substitution. Fluid substitution was performed on the dry rock moduli generated from the self-consistent model to uniform- and patchy-saturation cases. By comparing the differences of P-wave and S-wave velocities calculated for these cases, we can better understand the effect of fluid property changes for the Haynesville shale. For the dry pore case, moduli and density for pore fluids was zero. For patchy and uniform saturation, water saturation data from the well log was calculated by Archie's equation. Archie's equation is used to calculate water saturation in clean sandstone formations, so there might be errors in water saturation in the shale formation. Even though using water saturation calculated

by Archie's equation as input data in this simulation, it is assumed acceptable to analyze the effect of fluid property changes. I used the original XRD data composition and estimated pore aspect ratios by the velocity modeling for 50 Hz.

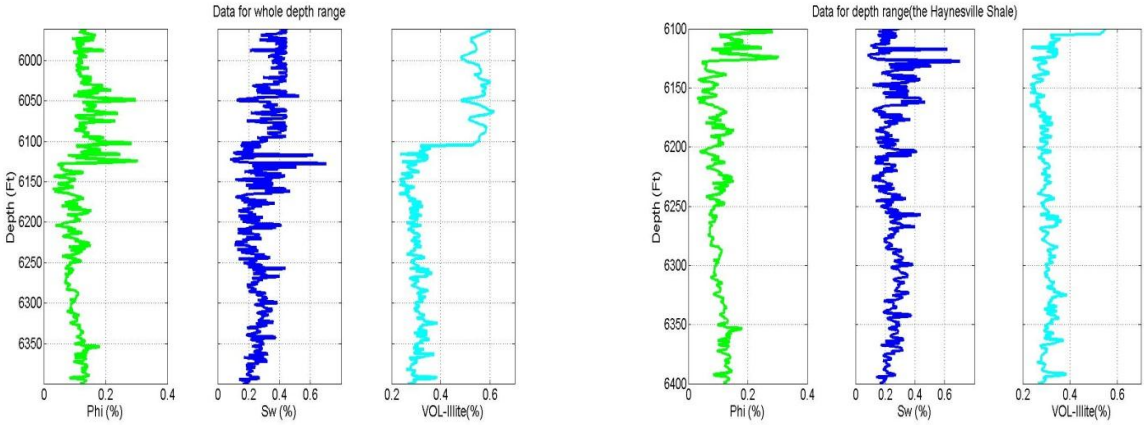

(a) (b)

Figure 15. Well log data. (a) the whole range of the well (b) the Haynesville Shale. In each figure, from the left, density porosity (%), water saturation (%), and volume of illite (%) are plotted versus depth. There is a large drop of volume clay content at the top of the Haynesville Shale relative to the overlying formation.

The water saturation for the Haynesville Shale varies from 0.0819 to 0.7020 with mean of 0.2462 from the well-log. By using this water saturation data, I calculated bulk moduli and densities for both patchy saturation and uniform saturation cases. Figure 16 shows bulk moduli and densities for both cases and constant values I used in the velocity modeling to estimate pore aspect ratios.

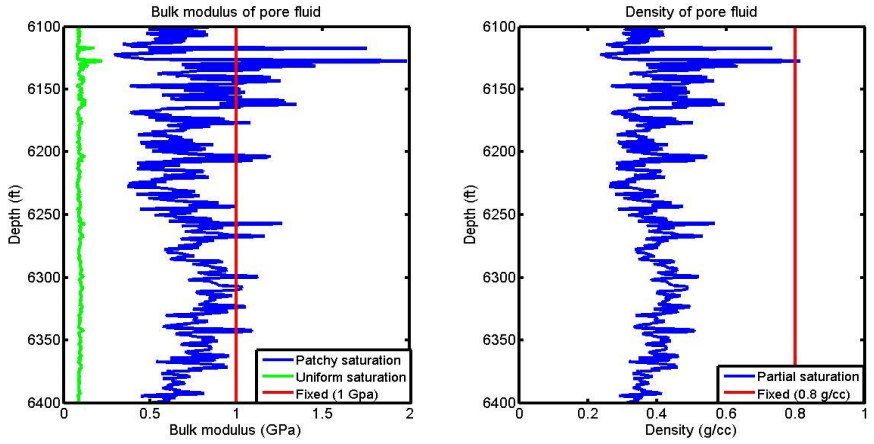

Figure 16. Bulk moduli and densities of fluids for patchy saturation, uniform saturation and fixed values (K_{fl}=1 GPa, density=0.8 g/cc for fluids) versus depth. Blue is for patchy saturation. Green is for uniform saturation. The red line is for the fixed value for the velocity modeling.

Velocity comparison by SCM for various types of fluid distributions

By setting bulk moduli and densities for pore fluids to zero within the self-consistent model, elastic moduli and velocities were calculated for dry rocks. Patchy and uniform cases were also calculated using the self-consistent model. Patchy saturation cases have the largest values for

bulk moduli, shear moduli, and P-wave velocities. Values for dry rock are the smallest and moduli for uniformly mixed fluids are in between them (Figure 17). Contrary to that, for the S-wave velocities, patchy saturation values are the largest, then, dry pore values, and uniform saturation values are the smallest at some depths. The reason that S-wave velocities of dry pore cases are larger than those of uniform saturation cases is because of the density effect in S-wave velocities. Bulk moduli and P-wave velocity graphs show similar patterns, and shear moduli and S-wave velocity graphs also show similar patterns in Figure 17. Comparing P-wave velocities and bulk moduli of patchy saturation to uniform saturation demonstrates patchy saturation values are much higher than uniform saturation values. This is not the case in graphs for S-wave velocities and shear moduli.

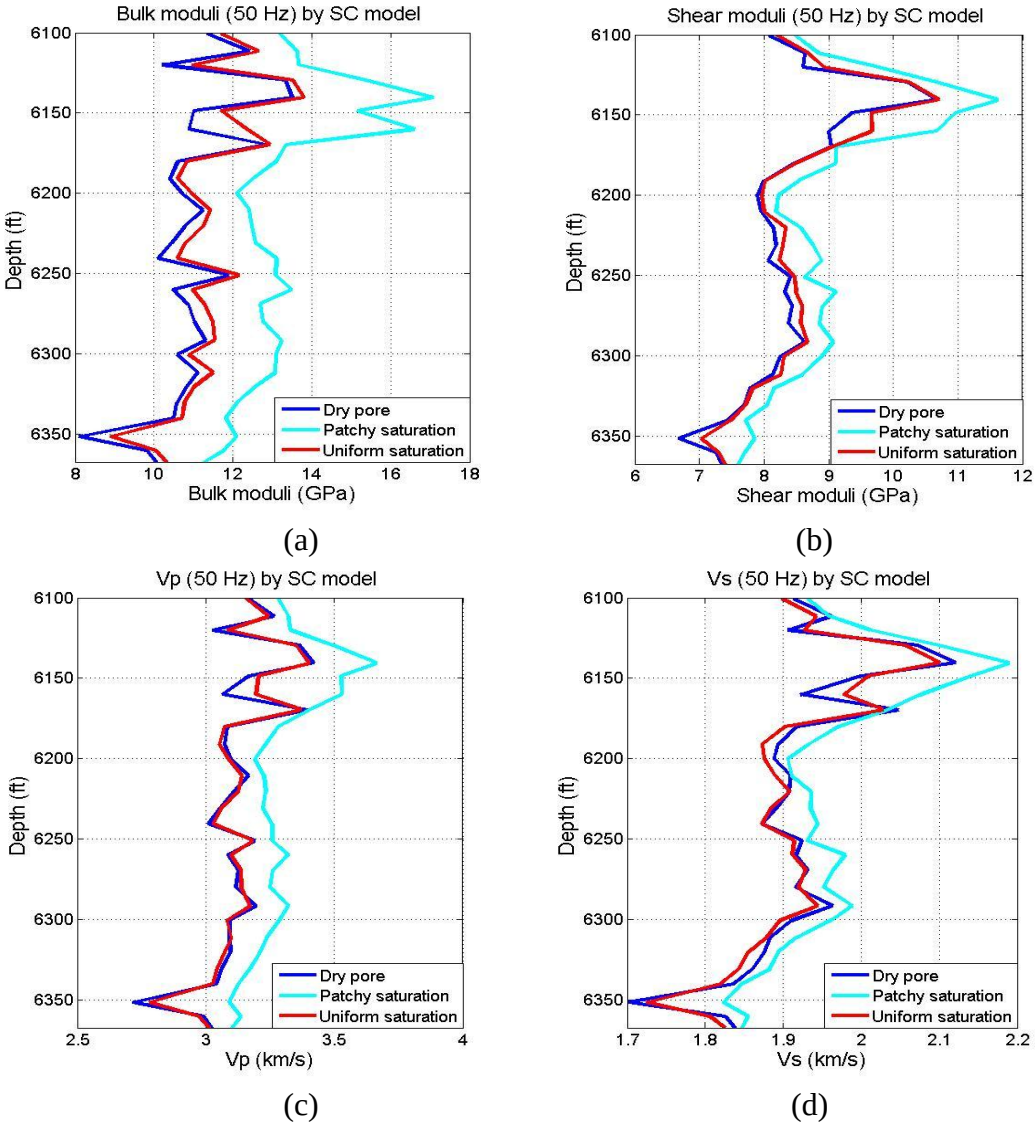

Figure 17. Graphs of (a) bulk moduli, (b) shear moduli (c) P-wave velocities, and (d) S-wave velocities for dry pores, the patchy and uniform saturation calculated by the self-consistent model for the Haynesville shale. Shear moduli and S-wave velocities for saturated cases are different from those of dry cases because the self-consistent model is a high-frequency model. Values between the patchy and uniform saturation are also different due to the effect of partial saturation.

When going from a dry- to fluid-saturated rock, the elastic bulk modulus of rock increases, and the bulk density also increases. However, the shear modulus of rock depends on the frequency of the model used. At low frequencies, the shear moduli of dry- and fluid-saturated rock are same according to Gassmann's relation. However, in inclusion-based models, the shear modulus of fluid-saturated rock increases with saturation changes compared to that of dry rock because the elastic-stiffening effect is exaggerated for both bulk and shear moduli. Velocities depend on the ratio of elastic moduli to density. According to the values of modulus and density, the velocities could increase or decrease. For the self-consistent approximation, local pore pressures increase in some pores and decreases in others, and there is no time to equilibrate. Therefore, the moduli and velocities increase due to frequency dispersion.

Velocity comparison by Gassmann substitution for various types of fluid distributions

Using Gassmann fluid substitution, I calculated P-wave and S-wave velocities for both the patchy and uniform saturation cases where the dry rock moduli were calculated from the self-consistent model. Before using Gassmann substitution, knowing the effective mineral moduli was necessary to study pore fluid effects. According to Jensen et al. (2011), a common strategy is to use the Hill average (Hill, 1963), which is the average of the Voigt bound and Reuss bound to obtain the effective solid properties.

Patchy saturation cases have the largest values for P-wave velocities calculated by Gassmann fluid substitution. Contrary to that, for the S-wave velocities, dry pore values are the largest, and the patchy and uniform saturation values are the same because Gassmann fluid substitution assumes shear modulus of fluid is zero. Adam et al. (2006) also indicated that Gassmann's theory predicts that the shear modulus will remain constant under different saturations. The reason that S-wave velocities of dry pore cases are larger than those of the patchy and uniform saturation cases is also the density effect in S-wave velocities. Very little difference exists for S-wave velocities of the dry cases versus the patchy and uniform saturation cases.

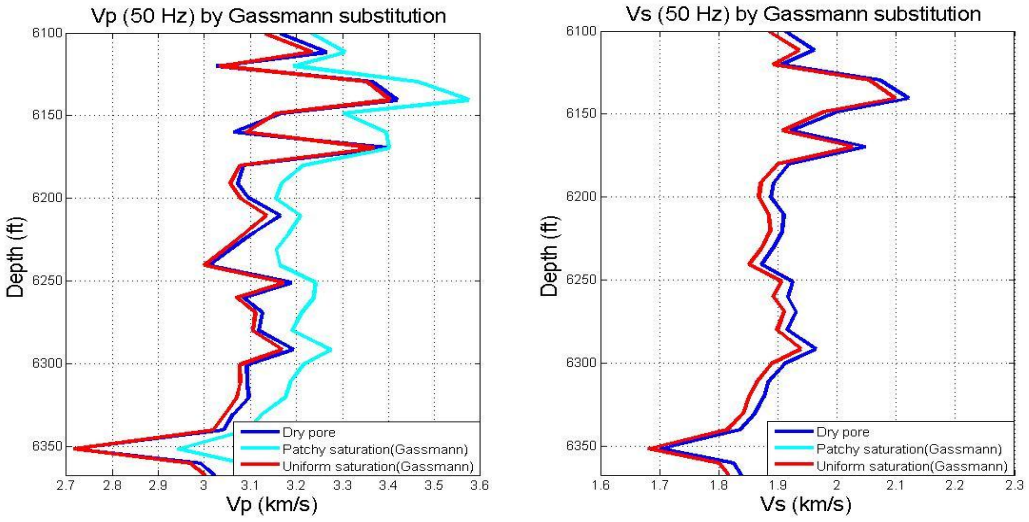

(a) (b)

Figure 18. Graphs of (a) P-wave velocities and (b) S- wave velocities for dry pores, the patchy and uniform saturation calculated by Gassmann fluid substitution for the Haynesville Shale. As expected, S-wave velocities for the patchy and uniform saturation cases are the same.

Velocity comparison between the self-consistent model and Gassmann fluid substitution

The self-consistent model calculates the effective elastic properties of rocks with multi-component minerals and various fluid-saturation cases by inputting elastic properties into the model directly. The pore inclusions in the self-consistent model are isolated with respect to fluid flow. Therefore, this model is appropriate for high frequency modeling of data. Whereas, Gassmann fluid substitution make it possible to calculate the bulk and shear moduli of the fluid-saturated rock from the dry rock mineral moduli at low frequency.

Knight et al. (1998) indicated that the relationship between elastic wave velocities and water saturation in a water/gas reservoir depends strongly on whether saturation is heterogeneous (patchy) or homogeneous (uniform). For patchy saturation cases, P-wave velocities from the self-consistent model are larger than the values from Gassmann fluid substitution, and the differences decrease in S-wave velocities in Figure 19. For uniform saturation cases, the differences of P-wave and S-wave velocities are very small. Because the self-consistent model is a high-frequency model, P-wave velocities from the model for the saturated rock should be different from P-wave velocities from Gassmann fluid substitution.

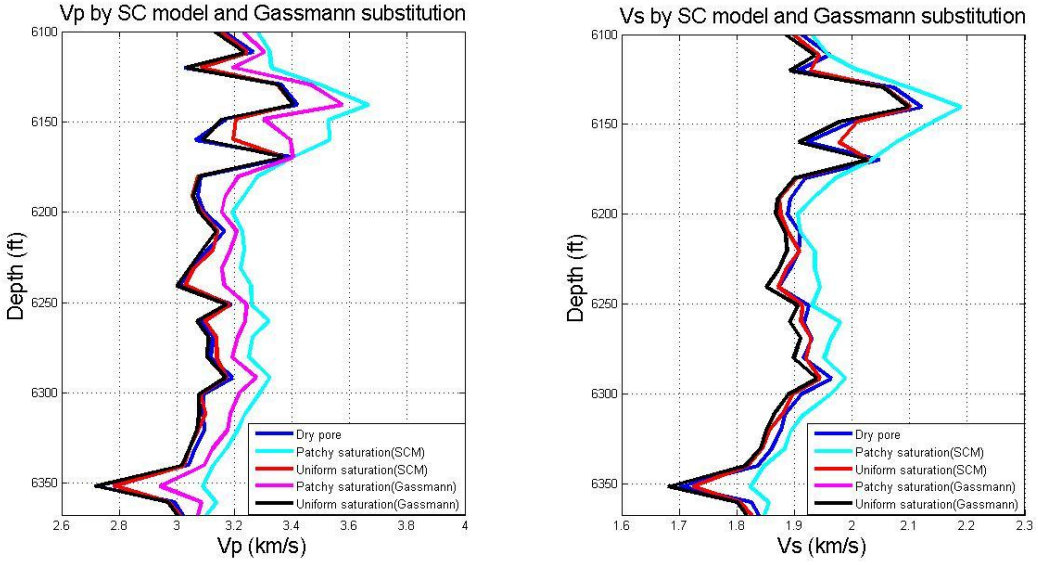

(a) (b)

Figure 19. Comparison of graphs of (a) P-wave velocities and (b) S-wave velocities for dry pores, the patchy and uniform saturation calculated by the self-consistent model and Gassmann fluid substitution for the Haynesville shale. S-wave velocities for the patchy and uniform saturation calculated by Gassmann fluid substitution are the same.

Results of velocity modeling for various types of fluid distributions

Pore aspect ratio estimation

In the first stage of study, P-wave velocities calculated from the self-consistent model were compared to up-scaled velocities using the moving Backus average to determine pore aspect ratios with fixed fluid properties. From the simulations of the effect of fluids, considerable P-wave velocity differences resulted according to the ways fluids were mixed. In this stage, I performed velocity modeling to determine pore aspect ratios for various fluid properties such as dry pores, the patchy saturation, and uniform saturation cases to analyze the effect of pore fluid mixing on determining pore aspect ratios. Aspect ratios currently are being computed from the Gassmann-derived velocities.

Pore aspect ratios for various fluid property types are plotted in Table 4 and Figure 20. Estimated pore aspect ratios of the interpolated data for the patchy saturation vary from 0.035 to 0.296 with the mean of 0.145. The range of pore aspect ratios of the interpolated data for the uniform saturation is from 0.051 to 0.319 with the average of 0.171 (Table 4). Estimated pore aspect ratios of the interpolated data for dry pores have the values from 0.052 to 0.310 with the mean of 0.168. Pore aspect ratios calculated for patchy saturation are the smallest values, then, dry pore values, and uniform saturation values are the largest. The graphs of estimated values for the patchy and uniform saturation in Figure 20 look very similar, but estimated pore aspect ratios for patchy saturation show the narrower range and smaller values than those of uniform saturation. In addition, it is evident that values from the interpolated data show more specific values and variations of pore aspect ratios versus depth compared to those from the XRD data in Figure 20.

	XRD data			Interpolated data		
	Dry pores	Patchy saturation	Uniform Saturation	Dry pores	Patchy saturation	Uniform Saturation
Max	0.298	0.298	0.308	0.310	0.296	0.319
Min	0.079	0.049	0.077	0.052	0.035	0.051
Mean	0.169	0.147	0.174	0.168	0.145	0.171

Table 4. The maximum, minimum and mean values of estimated pore aspect ratios for dry pores, the patchy and uniform saturation cases by velocity modeling (for 50 Hz).

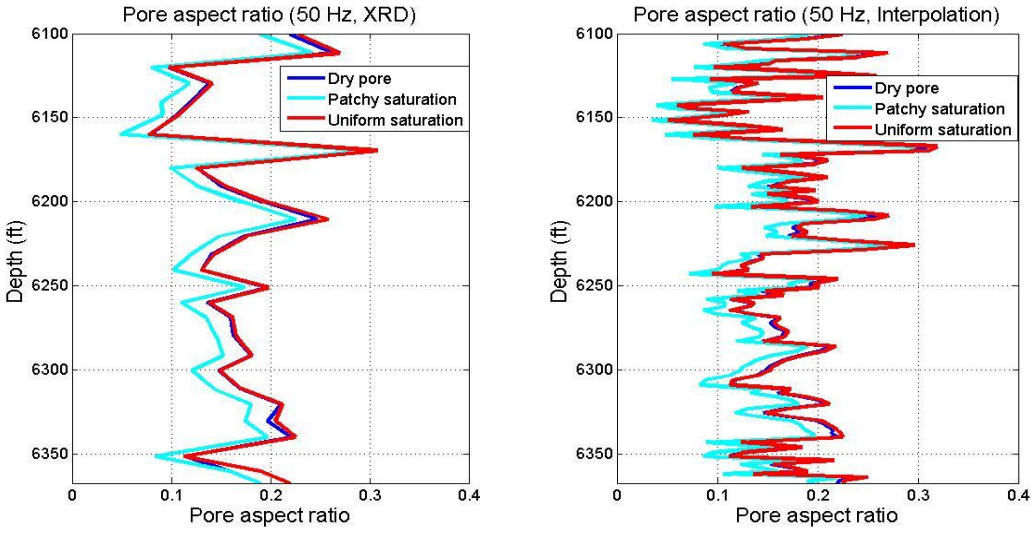

(a) (b)

Figure 20. Estimated pore aspect ratios for (a) XRD data, (b) Interpolated data for dry pores, the patchy and uniform saturation cases by using the self-consistent model and the Backus average (50 Hz) for the Haynesville Shale.

From the histograms in Figure 21, it is also possible to find the range of the pore aspect ratios for the various types of fluid properties. Contrary to that, for P-wave velocities calculated by the self-consistent model, patchy saturation cases have the largest values, then, uniform saturation cases, and dry pore values are the smallest. The histograms for the interpolated data appear to be normally distributed, but some of the histograms for the XRD data appear uniformly distributed.

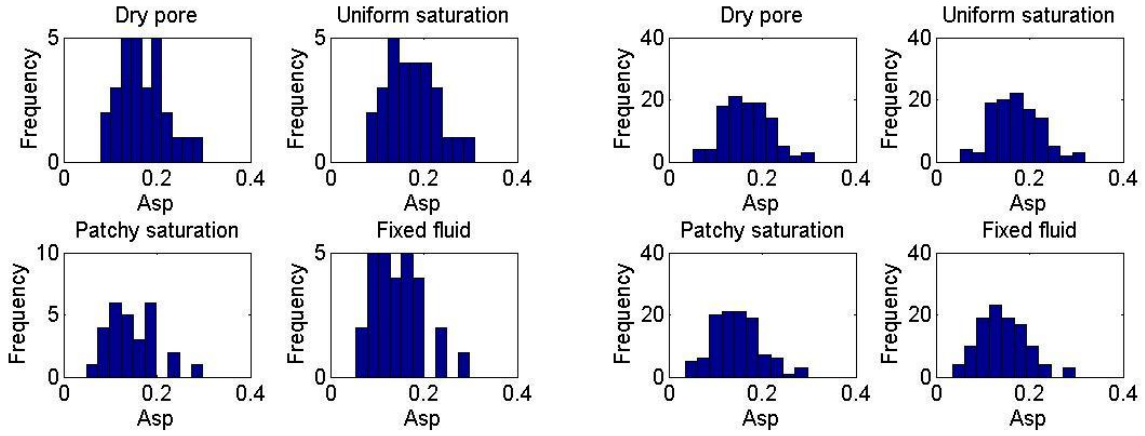

(a) (b)

Figure 21. Histograms of estimated pore aspect ratios for (a) XRD data, (b) Interpolated data for dry pores, fixed fluids, the patchy and uniform saturation cases by velocity modeling (for 50 Hz).

These results show quite different effects of fluid property types to pore aspect ratio determination and P-wave velocity calculation. It means fluid property types affect differently the calculations for pore aspect ratios and P-wave velocities in the self-consistent model. This is because of the modeling procedure used to determine pore aspect ratios in this study. For example, P-wave velocities calculated for the patchy saturation were higher than the uniform saturation and dry pores. In the modeling to determine aspect ratios of the pores, these P-wave velocities were used as one input variable. When these P-wave velocities calculated from the self-consistent model were compared to the Backus average, the differences of P-wave velocities between them increased because P-wave velocities for patchy saturation were higher than other fluid velocities. To make this difference below the criteria (0.5% P-wave velocity difference, Figure 11), the next estimated aspect ratio value had to be smaller than the current estimated value. Therefore, calculated aspect ratios for the patchy saturation were smaller than those of the uniform saturation and dry pores. It means that the calculation of velocities and pore aspect ratios are inversely related in the self-consistent model.

CONCLUSION

This study dealt with several practical topics to characterize reservoir properties of the Haynesville Shale. These include velocity modeling to determine pore aspect ratios and the effect of pore fluid property changes to P-wave and S-wave velocities. These methods could be applied to other gas shale formations where pore shape influences seismic velocity. To determine pore aspect ratios, P-wave velocities were compared from the self-consistent model and well data upscaled to the seismic scale. Determining pore aspect ratios using the velocity modeling helps us to understand elastic properties of the Haynesville Shale. This may help to find zones that correspond to optimal locations for fracturing the shale while considering brittleness and in-situ stress of the formation.

Velocity comparisons between the self-consistent model and Gassmann fluid substitution for dry pores, the patchy saturation and uniform saturation cases show that the scale and distribution of fluids affect the velocities. The relationship between elastic wave velocities and water saturation in a water/gas reservoir depends strongly on whether saturation is heterogeneous (patchy) or homogeneous (uniform). Especially for P-wave velocities, patchy saturation cases using the self-consistent model have the largest values compared to P-wave velocities calculated from Gassmann fluid substitution. In case of the uniform saturation, the differences of P-wave and S-wave velocities between two methods are much smaller than P-wave velocities for patchy saturation. From these comparisons, we can understand that elastic properties are strongly influenced by the fluid phase distributions in the pore space of the rock, and this affects the estimation of pore shape. These comparisons also show frequency-dependent characteristics. When going from a dry- to fluid-saturated rock, the elastic bulk modulus and bulk density increase. On the other hand, the shear modulus of rock depends on the frequency of the model used to calculate it. S-wave velocities calculated by the self-consistent model increase due to the frequency-related velocity dispersion and are different between the patchy and uniform saturation. However, S-wave velocities of the rock in Gassmann fluid substitution are same regardless of fluid mixture for the saturated rock because Gassmann substitution assumes that the shear modulus (G) remains unchanged between the dry rock and saturated rock. From these results, the shear moduli and S-wave velocities are sensitive to fluids at high frequencies whereas those at low frequencies are insensitive to fluids.

Estimated pore aspect ratios for various fluid mixtures were also calculated. Contrary to velocity comparisons, pore aspect ratios estimated for patchy saturation cases are the smallest and those for uniform saturation cases are the largest. These results show quite different effects of fluid property types to pore aspect ratio determination and P-wave velocity calculation. It means fluid property types affect differently the calculations for pore aspect ratios and P-wave velocities in the self-consistent model due to the modeling procedure used in this study. In the shale formation, gas originates from organic materials and migrates to the pore space. Clay-bound water is already saturated inside pores that are not connected with one another. Because there are large differences in elastic properties between water and gas, the mixing procedure for water and gas would be considered as a patchy saturation process. In conclusion, the pore aspect ratios determined for the patchy saturation cases are the most reasonable values for the Haynesville Shale.

ACKNOWLEDGMENTS

I would like to thank BP Inc. for providing the data, and I also thank Ursula Hammes for providing core analysis data. The EDGER Forum at the University of Texas at Austin supported this study.

REFERENCES

Adam, L., Batzle, M., and Brevik, I., 2006, Gassmann's fluid substitution and shear modulus variability in carbonates at laboratory seismic and ultrasonic frequencies, Geophysics, **71**, 173–183.

Avseth, P., Mukerji, T., and Mavko, G., 2005, Quantitative seismic interpretation: applying rock physics tools to reduce interpretation risk, Cambridge Univ. Press, Cambridge, England.

Avseth, P., Mukerji, T., Mavko, G., and Dvorkin, J., 2010, Rock-physics diagnostics of depositional texture, diagenetic alterations, and reservoir heterogeneity in high-porosity siliciclastic sediments and rocks - A review of selected models and suggested work flows, Geophysics, **75**, 75A31–75A47.

Backus, G. E., 1962, Long wave elastic anisotropy produced by horizontal layering, Journal of Geophysical Research, **67**, 4427-4440.

Bayuk, I. O., Ammerman, M., and Chesnokov, E. M., 2007, Upscaling of elastic properties of anisotropic sedimentary rocks, Geophysical Journal International, **172**, 842-860.

Berryman, J., 1980, Long-wavelength propagation in composite elastic media I. Spherical inclusions, Journal of the Acoustical Society of America, **68**, 1809-1819.

Berryman, J. G., Berge, P. A., and Bonner, B. P., 1999, Estimating rock porosity and fluid saturation using only seismic velocities, Stanford Exploration Project, **102**, 143–157.

Castagna, J. P. and Backus, M. M., 1993, Offset dependent reflectivity – theory and practice of AVO analysis, SEG, Investigations in Geophysics Series No. 8, Tulsa, OK.

Carmichael, R.S., 1989. Practical Handbook of Physical Properties of Rocks and Minerals., CRC Press, Boca Raton, FL.

Curtis, M. E., Ambrose, R. J., Sondergeld, C. H., and C. S. Rai, 2010, Structural characterization of gas shales on the micro-and nano-scales: Canadian Society for Unconventional Gas/Society of Petroleum Engineers, DOI: 10.2118/137693-MS.

Gassmann, F., 1951, On the elasticity of porous media, Vier. der Natur. Gesllschft in Zurich, **96**, 1-23.

Hammes, U., Eastwood, R., Rowe, H. D., and Reed, R. M., 2009, Addressing conventional parameters in unconventional shale-gas systems: depositional environment, petrography, geochemistry, and petrophysics of the Haynesville Shale: 29th Annual GCSSEPM Foundation Bob F. Perkins Research Conference, Houston, 181–202.

Hammes, U., Hamlin, H. S., and Ewing, T. E., 2011, Geologic analysis of the Upper Jurassic Haynesville Shale in east Texas and west Louisiana, AAPG Bulletin, **95**, 1643-1666.

Hill, R., 1963. Elastic properties of reinforced solids: some theoretical principles. J. Mech. Phys. Solids, **11**, 357–372.

Jensen, E. H., Andersen, C. F., and Johansen, T. A., 2011, Estimation of elastic moduli of mixed porous clay composites, Geophysics, **76**, E9-E20.

Jiang, M and Spikes, K., 2011, Pore-shape and composition effects on rock-physics modeling in the Haynesville Shale, 2011 SEG Annual Meeting, San Antonio, TX.

Knight, R., and Nolen-Hoeksema, R., 1990, A laboratory study of the dependence of elastic wave velocities on pore scale fluid distribution, Geophysics, **17**, 1529-1532.

Knight, R., Dvorkin, J., and Nur, A., 1998, Acoustic signatures of partial saturation, Geophysics, **63**, 132–138.

Mavko, G., Mukerji, T. and Dvorkin, J., 2009, The rock physics handbook (2nd Edn), Cambridge Univ. Press, Cambridge, England.

Mavko, G., and Mukerji, T., 1998, Bounds on low-frequency seismic velocities in partially saturated rocks, Geophysics, **63**, 918-924.

Simmons, G., and Birch, F., 1963, Elastic constants of pyrite, J. Appl. Phys., **34**, 2736-2738.

Sondergeld, C. H., Ambrose, R. J., Rai, C. S., and Moncrieff, J., 2010, Micro-Structural Studies of Gas Shales, 2010 SPE Unconventional gas Conference, Pittsburgh, Pennsylvania.

Sun, Y. F., 2004, Pore structure effects on elastic wave propagation in rocks: AVO modeling, Journal of Geophysics and Engineering, **1**, 268–276.
Wilks, D. S., 2011, Statistical methods in the atmospheric sciences (3rd Edn), Elsevier Inc., Oxford, England.